RESEARCH

Application of ZnO nanorods as an adsorbent material for the removal of As(III) from aqueous solution: kinetics, isotherms and thermodynamic studies

Gutha Yuvaraja[1] · Cheera Prasad[2] · Yarramuthi Vijaya[3] · Munagapati Venkata Subbaiah[4]

Abstract

Removal of metals from wastewaters causes a big concern from the environmental point of view due to their extreme toxicity towards aquatic life and humans. Application of As(III) from aqueous solution by ZnO nanorods as adsorbent has been investigated in the present study. The synthesized nanorods were characterized by XRD, FT-IR spectroscopy, SEM, and thermogravimetric analysis. Optimum biosorption conditions were determined with respect to pH, adsorbent dose, contact time, and temperature. The experimental data were examined using the Lagergren's first-order, pseudo-second-order and intraparticle diffusion kinetic models. The results revealed that the pseudo-second-order kinetic model provided the best description of the data. Langmuir and Freundlich isotherm models were applied to the equilibrium data. The maximum As(III) sorption capacity of ZnO nanorods was found to be 52.63 mg/g at pH 7, adsorbent dose 0.4 g, contact time 105 min, and temperature 323 K. The calculated thermodynamic parameters, ΔG^o (between -5.741, -5.342 and -4.538 kJ/mol at 303–323 K), ΔH^o (13.75 kJ/mol) and ΔS^o (0.0616 J/mol K) showed that the sorption of As(III) onto ZnO nanorods was feasible, spontaneous and exothermic, respectively.

Keywords ZnO nanorods · As(III) · Kinetics · Isotherms · Thermodynamics

Introduction

Water pollution due to the release of various toxic chemicals and dyes from industrialization and urbanization is a global problem [1–31]. Arsenic occurs naturally in the earth's crust, and much of its dispersion in the environment stems from mining and commercial uses. In industry, arsenic is a byproduct of the smelting process (separation of metal from rock) for many metal ores such as zinc, lead and cobalt. It

cannot be destroyed once it has entered the environment, so that the amounts that we add can spread and cause health effects to humans and animals. The effects of arsenic exposure include discoloration of the skin, gangrene, intestinal problems, and carcinogenic effects include skin, lung, liver, kidney, and bladder cancers and ultimately death [32]. To reduce the health risks of human beings, the U.S. Environmental Protection Agency (USEPA) revised the maximum contaminant level (MCL) for arsenic in drinking water from 50 to 10 µg/L [33].

Arsenic occurs in the environment in several oxidation states such as -3, 0, $+3$ and $+5$. Inorganic arsenic is generally found as trivalent arsenite or pentavalent arsenate form in the aqueous solution. As(III) is a hard acid and preferentially complexes with oxides and nitrogen. Whereas As(V) behaves like a soft acid, forming complexes with sulfides [34]. The speciation of arsenic in water is usually controlled by redox conditions, pH, biological activity, and adsorption reactions [35, 36]. As(III) is more toxic than As(V) and it is very difficult to remove from water. As a result of heightened guideline of arsenic toxicity and regulatory

✉ Gutha Yuvaraja
   yuvaraj.svu@gmail.com

1 Tianjin University Chemical Engineering Research Center, Tianjin University, Tianjin 300072, China

2 Biopolymers and Thermo Physical Laboratories, Department of Chemistry, Sri Venkateswara University, Tirupati 517 502, Andhra Pradesh, India

3 Department of Chemistry, Vikrama Simhapuri University, Nellore 524-003, Andhra Pradesh, India

4 Department of Environmental Science and Engineering, Ewha Womans University, 11-1 Daehyun-Dong, Seodaemun-Gu, Seoul 120-750, Korea

∅ Springer

changes, prompting innovative research efforts towards efficient removing arsenic from contaminated water is of critical importance.

Many technologies such as coagulation [37], ion exchange [38], membrane filtration [39, 40], and precipitation [41] have been employed for the removal of metal ions from aqueous solutions and effluents. However, these methods can prove to be too costly, impractical to apply over large scales, or unable to remove trace quantities of the metalloid. To overcome these drawbacks, adsorption is a good alternative to remove metal ions from aqueous environment. Different types of adsorbents [42–49] have been used for the removal of a variety of pollutants from water. Recently, the application of nanomaterials, nanoadsorbents has come forth as a fascinating area of interest for the removal of metallic and dye pollutants from water [50–53]. A variety of nanoparticles titanium dioxide suspensions [54], chitosan nanoparticles [55], zinc oxide nanoparticles [56], Nickel/nickel boride nanoparticles-coated resin [57], zirconium oxide nanoparticles [58], $MnFeO_4$ and $CoFe_2O_4$ [59] have been used for the removal of metal ions from water. Nanoparticles are having high adsorption capacity due to its large surface area. In this connection, utilization of nanoparticles has greater attention in metal ion removal process. As per the literature survey, there are no studies on the adsorption of As(III) using ZnO nanorods. Therefore, in the present study, ZnO nanorods have been used for the removal of As(III) from aqueous solution.

The goal of this work is to investigate the sorption capacity of ZnO nanorods as an adsorbent for the removal of As(III) from aqueous environment. The effects of varying parameters such as pH, dose, initial metal concentration, contact time and temperature on the adsorption process were examined. To clarify the sorption kinetics of As(III) by ZnO nanorods, Lagergren's pseudo-first-order, pseudo-second-order and intraparticle diffusion models were applied to the experimental data. The isotherms of adsorption have been studied and various isotherm models, such as Langmuir, and Freundlich models, have been tested. In addition, thermodynamic parameters including the change in free energy (ΔG^o), enthalpy (ΔH^o) and entropy (ΔS^o) were calculated to evaluate the thermodynamic behavior of the biosorption process.

Materials and methods

Materials

All the reagents were of analytical grade with a purity of 99% and used as received without further purification. $ZnSO_4 7H_2O$ (S. D. Fine chemicals limited), KOH (Qualigens fine chemicals) tetraethyl orthosilicate (Sigma Aldrich). The glassware used was soaked in 10% HNO_3 overnight before use and cleaned repeatedly with double distilled water. The stock solutions of As(III) were prepared by dissolving As_2O_3 in double distilled water. Fresh dilutions were used for each study. The initial pH of each solution was adjusted with 0.1 M HCl and NaOH.

Synthesis of ZnO nanorods

ZnO nanoparticles were prepared by drop by drop addition of 0.3 M of KOH (19.03 g/100 mL) from a burette to 0.017 M solution of $ZnSO_4 H_2O$ (5 g/100 mL) with constant stirring (500 rpm). The reaction mixture was stirred at room temperature. Then, tetraethyl orthosilicate (capping agent) was added in a certain amount to the reaction mixture to inhibit the growth of zinc hydroxide crystallite during the course of the precipitation. The solution becomes milky white under the constant stirring. The precipitate is separated by the filtration. After that, it washed several times with distilled water and absolute methanol until the impurities are free from precipitate. Finally, it was dried in hot air oven for 1 h at 353 k. The ZnO nanorods were stored in airtight containers and kept in desiccators until further use.

Apparatus

The crystallinity and phase identification of adsorbent powders were determined by X-ray diffraction (XRD) using a Rigaku Ultima III system equipped with a Cu sealed tube ($\lambda = 1.54178°A$). FT-IR spectra of the pure, As(III) loaded ZnO nanorods were measured with an FT-IR spectrophotometer (Thermonicolet-200 series, Germany) under ambient conditions. The spectra were recorded from (4000 to 500 cm^{-1}) using a KBr pellet. The surface morphology of the samples was observed Scanning electron micrographs (Carl Zeiss, EVO MA 15, England). The pH of the As(III) solution is measured with a digital pH meter (Digisum D1-7007, India). Thermal gravimetric analysis (TGA) was carried out using on a Linseis L81-I TG–DTA instrument with a heating rate of 10 °C min^{-1} under an N_2 atmosphere.

Batch adsorption studies

To obtain the performance of sorbent material, batch experiments were conducted. The pH of the solutions was adjusted by adding 0.1 M HCl and NaOH. A total of 0.4 g of adsorbent (ZnO nanorods) was mixed with 50 mL of As(III) solution in 125 mL of Erlenmeyer flasks. The pH of the solutions was adjusting by 0.1 M of HCl or NaOH. Then, the flasks were shaken at room temperature (303 K) for 2 h to reach equilibrium in shaking incubator. After that the samples were withdrawn from the shaking incubator and filtered through whatman filter paper 41 to remove As(III) from the

solution. The amount of As(III) ions in the filtered solution was estimated.

$$q_e = \frac{(C_i - C_e)V}{M} \tag{1}$$

where q_e (mg/g) was the adsorption capacity at equilibrium, C_i and C_e are initial and equilibrium concentration (mg/L) of As(III) in the aqueous phase, respectively, M (g) is the biosorbent dosage, and V (L) is the volume of the aqueous phase.

Results and discussion

Characterization of the adsorbent material

XRD analysis

XRD spectra of pure and As(III) loaded ZnO nanorods are shown in Fig. 1. The peaks were seen at 31.96, 34.62, 36.44, 47.74, 56.79 and 63.05, which can be assigned to diffraction from (100), (002), (101), (102), (110) and (103) planes, respectively. This revealed that the resultant nanoparticles were of pure zinc oxide with a hexagonal structure.

FT-IR analysis

The functional groups of the synthesized ZnO nanorods were analyzed using the FT-IR spectrum. FT-IR spectra of pure and As(III) loaded ZnO nanorods are shown in Fig. 2. The major bands for the ZnO nanorods can be assigned as follows: The broad and strong bands at 3378 cm^{-1} (are due to the overlapping of –OH and –NH$_2$ stretching vibrations), 1659 cm^{-1} (–NH$_2$ bending
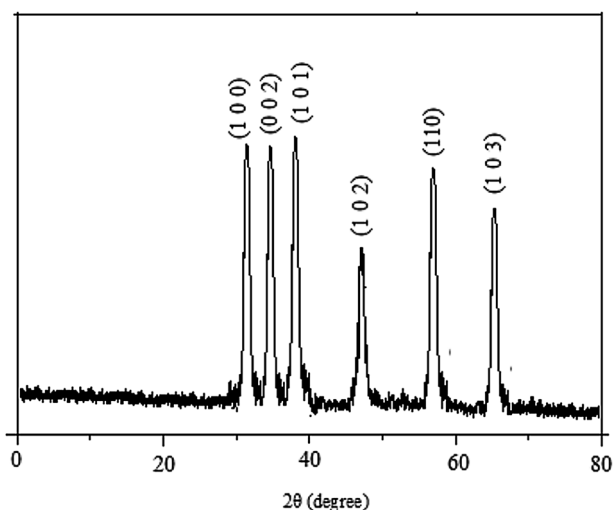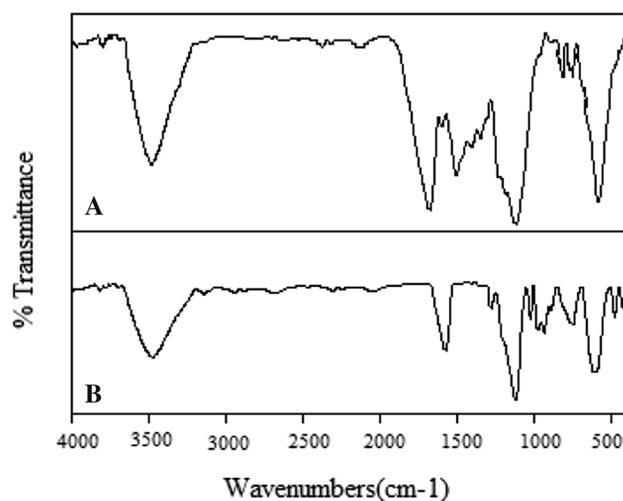

Fig. 1 X-RD spectra of pure ZnO nanorods

Fig. 2 FT-IR spectra of **a** pure ZnO nanorods and **b** As(III)-loaded ZnO nanorods

vibrations), 1370 cm^{-1} (–CH symmetric bending vibrations in ZnO–OH), 1019 cm^{-1} (–CO stretching vibration in –COH). In addition, a broad absorption peak about 400–590 cm^{-1} was assigned to the inorganic Zn–O stretching band. After As(III) loaded, the broad band at 3415 cm^{-1} which is concerned with –OH and –NH$_2$ stretching vibrations increases after sorption process. This may be attributed to the deformation of –OH and –NH$_2$ bands as a result of interaction between the functional groups and metal ions. The intensity of the band at 1659 cm^{-1} is substantially decreased to 1618 cm^{-1} after As(III) loaded. The shift of the peak from 1019 to 1032 cm^{-1} suggests the involvement of the C–O group in binding As(III).

SEM analysis

Surface morphology of the adsorbent is the most important one and the adsorption capacity mainly depends on the surface structure and surface porosity. Figure 3 shows the SEM images of (a) ZnO nanorods and (b) As(III)-loaded ZnO nanorods. From Fig. 3a, it is clearly observed that the pure ZnO nanorods are formed. After As(III) loaded (Fig. 3b), the nanorods are fully covered with the metal. It can be observed that the surface morphologies of ZnO are different before and after As(III) loaded.

TGA analysis

The TGA graph (Fig. 4) shows weight loss up to 450 °C and after this point there was no significant weight loss detected. The first weight loss occurred at 120 °C, representing the
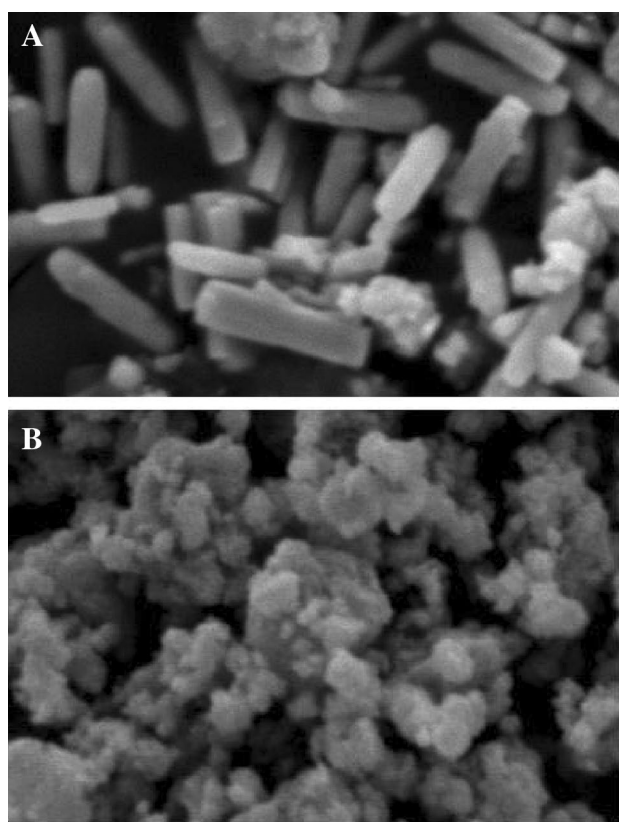
Fig. 3 SEM images of **a** pure ZnO nanorods, **b** As(III)-loaded ZnO nanorods
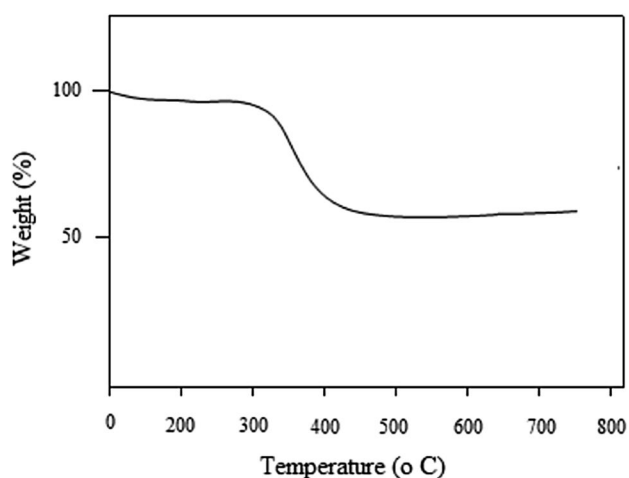
Fig. 4 TGA graph of ZnO nanorods

dehydration of samples due to desorption of physically adsorbed water molecules on the surface of ZnO nanorods. The second weight loss occurred between 250 and 350 °C, indicating the loss of OH^- and CO_3^{2-}.

Influence of solution pH

The pH of the solution is considered to be one of the most important factors affecting the biosorption process. The pH affects not only the solution chemistry of the metals but also the ionization state of the functional groups present on the surface of the sorbent. The effect of initial pH on the biosorption of As(III) onto ZnO nanorods was evaluated within the pH range of 2–9 (Figure not shown). At low pH values, protons occupy most of the sorption sites on the sorbent surface and less As(III) could be sorbed because of electrostatic repulsion. When the pH values increased, adsorbent surfaces were more negatively charged and the sorption of metal ions (positive charge) increased and reached maximum at pH 7.0 for As(III). Decreased sorption at higher pH (pH > 7.0) was due to the formation of soluble hydroxylated complexes of the metal ions and their competition with the active sites, and as a consequence, the retention had been decreased again. For this reason, the optimum pH was selected to be 7.0 for further experiments.

The effect of pH can also be explained in terms of pH_{pzc} of the biosorbent. The pH_{PZC} is an important characteristic for adsorbents to determine the pH at which the surface has net electrical neutrality. The initial pH of each solution was adjusted with 0.1 M HCl and NaOH. At pH < PZC, the surface charge of the adsorbents is positive which results in low As(III) sorption. At pH > PZC, the surface charge of the adsorbents is negative and the As(III) ions in solution were attracted to the surface to a greater extent. The PZC value of the ZnO nanorods is found to be 6.5.
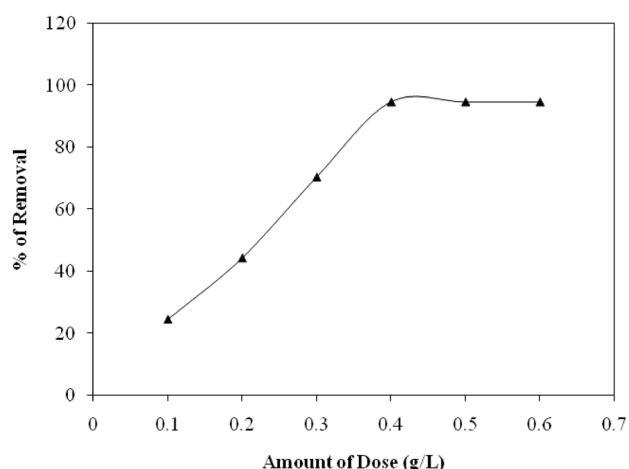
Effect of agitation speed

The agitation speed experiments were undertaken with different agitation speeds of (30, 60, 90, 120, 150, 180, and 210) rpm keeping constant the other process variables. The amount of As(III) adsorption increases with an increase of the agitation speed from (30 to 210) rpm and the highest amount of As(III) (96% removal and the figure was not shown) was obtained with an agitation speed of 180 rpm. Lower speeds probably caused inefficient dispersion of adsorbent particles in water that led to agglomeration of particles. At higher agitation speed (> 180 rpm), the As(III) amount decreases. Hence, the optimum speed of 180 rpm has been selected for further study.

Influence of adsorbent dose

The amount of the adsorbent is an important parameter because it determines the adsorption capacity of an adsorbent for a given initial concentration of the adsorbate. The effect of adsorbent dose has been studied with various amounts of sorbent (0.1–0.6 g), while keeping all the other

Fig. 5 Effect of adsorbent dose for the removal of As(III) from aqueous environment

parameters constant at their optimum values (i.e., pH, agitation speed, temperature and contact time). From results (Fig. 5), the removal percentage of As(III) increases with increasing higher dosages. This is attributed to the increased adsorbent surface area and more available adsorption sites or functional groups because of the increase in adsorbent quantity. Beyond 0.4 g, there was no appreciable increase in the percentage adsorption, which indicates the saturation of the active adsorption sites in the biopolymer composite. An adsorbent content of 0.4 g was selected for all further experiments because of the high adsorption efficiency and acceptable adsorption capacity at this value.

Influence of initial metal ion concentration and contact time

Contact time is one of the important parameters for successful biosorption application. To examine the effect of the initial metal concentration, the biosorption experiments were carried out at different initial metal concentrations (30, 50, 70, and 90 mg/L) at the optimum temperature and pH. The initial As(III) ion concentration was varied (30–90 mg/L) with varying contact times (15–120 min). The removal percentage increases with increasing the metal

ion concentration (Figures not shown) and then it remained unchanged by further increase in initial metal ion concentrations. These results suggest that the available sites on the biosorbent are the limiting factor for the As(III) adsorption. It was observed that the sorption process reached equilibrium at 105 min. Afterwards, there were no significant changes in As(III) onto ZNO nanorods. Hence, the contact time of 105 min is selected for As(III) ions for further studies.

Kinetic models

Adsorption kinetics is important from the point of view that it controls the efficiency of the process and the models correlate the adsorbate uptake rate with its bulk concentration.

To analyze the adsorption rate, pseudo-first-order [60], pseudo-second-order [61] and intraparticle diffusion models [62] were used to investigate the adsorption kinetics of As(III) onto the ZnO nanorods.

The linear form of pseudo-first-order rate equation is generally expressed as follows:

$$\log (q_e - q_t) = \log q_e - \frac{K_1}{2.303}t \tag{2}$$

where q_e (mg/g) and q_t (mg/g) are the amounts of As(III) sorbed at equilibrium and at time t. K_1 (min^{-1}) is the rate constant of first-order biosorption process. The pseudo-first-order kinetic constants were determined from slope of the plot of $\log (q_{e-} q_t)$ versus t (Figure not shown) and the values are shown in Table 1.

The pseudo-second-order kinetic model of McKay and Ho can be expressed as:

$$\frac{t}{q_t} = \frac{1}{K_2 q_e^2} + \frac{1}{q_e}t \tag{3}$$

where q_e and q_t are the amount of the As(III) removal per unit mass of biosorbent (mg/g) at equilibrium and at time t (min), and K_2 (g/mg.min) is the pseudo-second-order rate constant. The biosorption rate constant (K_2) is obtained from linear plot of t/q_t versus t (Figure not shown) and the values are included in Table 1. As shown in Table 1, the R^2 values for pseudo-second-order kinetic model at all the

Table 1 Kinetic parameters for the removal of As(III) onto ZnO nanorods at different As(III) concentrations

As(III) Conc. (ppm)	Pseudo-first-order			Pseudo-second-order			Weber and Morris		
	K_1 (1/min)	R^2	SSE	K_2 (g/mg min)	R^2	SSE	K_{id} (mg/g min$^{-0.5}$)	R^2	SSE
30	0.020	0.995	0.973	0.0087	0.999	0.1844	0.142	0.986	0.8197
50	0.027	0.992	0.971	0.0091	0.999	0.1272	0.171	0.977	0.4768
70	0.029	0.986	0.978	0.0058	0.989	0.1477	0.251	0.975	0.3319
90	0.036	0.959	0.985	0.0087	0.999	0.0303	0.336	0.941	0.1852

concentrations studied are higher than pseudo-first-order model. It was suggested that the pseudo-second-order model is more suitable for describing the sorption of As(III) onto ZNO nanorods.

The intraparticle diffusion model is based on the theory proposed by Weber and Morris

$$q_t = K_{id}t^{0.5} + c \tag{4}$$

where q_t (mg/g) is the amount adsorbed at time t (min), K_{id} is the intraparticle diffusion rate constant (mg/g min$^{-0.5}$) and C is the intercept that gives an idea about the thickness of the boundary layer. The intraparticle diffusion model coefficient values are calculated from the plot of q_t versus $t^{0.5}$ (Figure not shown) and are given in Table 1. It can be deciphered that these plots of q_t versus $t^{0.5}$ have three distinct regions. The initial region of the curve relates the adsorption on the external surface. The second region corresponds to the gradual uptake, which reflects the intraparticle diffusion as the rate-limiting step. The final plateau region indicates the equilibrium uptake. It denotes that the intraparticle diffusion is not the only rate-controlling step.

In addition, the sum of square error (SSE) test was carried out to predict the best fit.

$$SSE = \sum \frac{(q_{t,e} - q_{t,m})^2}{q_{t,e}^2} \tag{5}$$

where $q_{t,e}$ and $q_{t,m}$ are the experimental biosorption capacities of metal ions (mg/g) at time t and the corresponding values that are obtained from the kinetic models. SSE values for all kinetic models are calculated and are summarized in Table 1. Pseudo-second-order model has the lowest SSE values when compared with the pseudo-first-order and intraparticle diffusion models. Based on the low SSE values, it can be concluded that biosorption As(III) onto ZNO nanorods follows pseudo-second-order model.

Equilibrium isotherms

The capacity of an adsorbent can be described by sorption isotherms, which can help to explore the adsorption mechanism much more thoroughly. The sorption data have been subjected to different sorption isotherms, namely the Langmuir [63] and Freundlich [64].

The Langmuir model assumes that the uptake of metal ions occurs on a homogeneous surface by monolayer adsorption without any interaction between adsorbed ions. The linearized form of this isotherm can be expressed as:

$$\frac{1}{q_e} = \frac{1}{q_m K}\left[\frac{1}{C_e}\right] + \frac{1}{q_m} \tag{6}$$

where q_e is the equilibrium metal ion concentration on the sorbent (mg/g), C_e is the equilibrium metal ion concentration in the solution (mg/L), q_m is the monolayer biosorption capacity of the sorbent (mg/g), and K is the Langmuir constant related to the free energy of sorption.

As seen from Table 2 the R^2 values indicates that the Langmuir isotherm model fits well to the experimental data. The maximum adsorption capacity q_{max} was calculated from the Langmuir equation indicating the q_{max} of As(III) with ZnO nanoparticles 52.63 mg/g, respectively. For the Langmuir isotherm, a dimensionless separation factor can be expressed by the following equation:

$$R_L = \frac{1}{(1 + bC_0)} \tag{7}$$

where b is the Langmuir constant (L/mg) and C_o is the initial biosorbent concentration of As(III) ions (mg/L). The value of R_L indicates the shape of isotherm to be either unfavorable ($R_L > 1$), Linear ($R_L = 1$), Favorable ($0 < R_L < 1$), or irreversible ($R_L = 0$). In this study, the R_L values lie between 0 and 1. This indicates that the biosorption of As(III) onto ZNO is favorable.

The Freundlich isotherm is used for modeling the biosorption of metal ions on heterogeneous surfaces and the linearized form of the isotherm is as follows:

$$\log q_e = \log K_f + \frac{1}{n}\log C_e \tag{8}$$

where K_f (mg/g) is a constant relating the biosorption capacity and $1/n$ is an empirical parameter relating the biosorption intensity. The values of Freundlich constants K_f and $1/n$ are included in Table 2. The values of Freundlich constants K_f and $1/n$ were obtained from the plots of $\log C_e$ versus $\log q_e$ (Figure not shown) and the values are included in Table 2. It is clear that the R^2 values are not closer to unity compared to Langmuir model. This value indicates the degree of nonlinearity between solution concentration and adsorption as

Table 2 Langmuir and Freundlich isotherm constants and correlation coefficients for the removal of As(III) onto ZnO nanorods at different temperatures

Temp. (K)	Langmuir isotherm				Freundlich isotherm			
	q_m (mg/g)	K_L (L/mg)	R^2	χ^2	K_f (mg/g)	$1/n$	R^2	χ^2
303	38.46	9.76	0.999	4.34	9.79	0.471	0.990	25.30
313	41.66	7.79	0.999	6.32	9.84	0.510	0.993	24.70
323	52.63	5.42	0.999	14.11	6.50	0.617	0.996	54.78

follows: if $n = 1$, then adsorption is linear; if $n < 1$, then adsorption is a chemical process; if $n > 1$, then adsorption is a physical process. The n value in Freundlich equation was found to be 2.12, 1.96, and 1.62 for ZnO nanorods at three different temperatures (303, 313 and 323 K). Since n lie between 1 and 10, this indicates the physical adsorption of As(III) onto ZnO nanorods.

Chi square (χ^2) analysis

Chi square (χ^2) test was adopted to find the suitability of an isotherm that fits best the experimental data. The Chi square (χ^2) statistics is basically the sum of the squares of the difference between the experimental and calculated data from models, with each squared difference divided by corresponding data obtained by calculation. The equation for evaluating the best fit model is as follows:

$$\chi^2 = \sum \frac{(q_e - q_{e,m})^2}{q_{e,m}} \tag{9}$$

where $q_{e,m}$ is the equilibrium capacity obtained from the model (mg/g) and q_e is the experimental equilibrium capacity (mg/g). From Table 2, lower χ^2 values of Langmuir isotherm model show that the experimental data correlate well with the Langmuir isotherm than the Freundlich isotherm.

Effect of temperature

Temperature plays key roles on the biosorption process. Biosorption experiments were conducted at 303, 313 and 323 K to investigate the effect of temperature, with initial As(III) concentration of 125–225 mg/L, adsorbent dosage of 0.4 g/L, pH 7 and contact time of 105 min. It was observed that the maximum adsorption capacity of As(III) ion reached up to 52.63 mg/g at 323 K. The sorption capacity increased when temperature of the solution was increased, indicating that the process was endothermic. This may be a result of an increase in the mobility of As(III) ions with increasing temperature. An increasing number of molecules may also acquire sufficient energy to undergo an interaction with active surface sites of the adsorbent.

Thermodynamic parameters, such as of Gibbs free energy change (ΔG^o), enthalpy change (ΔH^o) and entropy change (ΔS^o), were used to evaluate the thermodynamic feasibility of the process and to confirm the nature of the biosorption process. The parameters were determined using the following equations:

$$\Delta G^o = -RT \ln K_L \tag{10}$$

$$\ln K_L = -\frac{\Delta H^o}{RT} + \frac{\Delta S^o}{R} \tag{11}$$

Table 3 Comparison of adsorption capacity of various adsorbents for As(III) ions from aqueous solution

Adsorbent	Adsorption capacity (q_{max}) mg/g	Reference
Biochar (derived from rice husk)	19.3	[17]
Fe7S8 nanoparticles	14.3	[65]
Fe-SM (iron-coated S. muticum)	4.2	[66]
Calix [4] pyrrole	15.28	[67]
CeeFe mixed oxide MWCNT	28.74	[68]
Zero valent iron/mesoporous carbon	26.8	[69]
Activated carbon–alumina composites	14.28	[70]
ZnO nanorods	52.63	Present study

where R is the universal gas constant (8.314 J/mol K), T is the temperature (K) and K is obtained by multiplying Langmuir constant b and q_m. The negative values (-5.741, -5.342 and -4.538 kJ/mol) of ΔG^o indicate the spontaneous nature the adsorption of AS(III) at (303, 313, 323 K), respectively. The positive ΔH^o value (13.75 kJ/mol) suggested that the AS(III) adsorption is endothermic in nature. The positive ΔS^o value (0.0616 J/mol K) reveals the increase in randomness at the solid-solution interface during the fixation of the antimony ion on the active sites of the adsorbent.

Comparison of ZnO with other adsorbents

Table 3 shows a comparison of the maximum adsorption capacity of different materials reported in the literatures [17, 65–70] as adsorbents for As(III) from aqueous media under different experimental conditions. The q_{max} (52.63 mg/g) value of for ZnO nanorods was much higher than those materials used for removing As(III) ions. Also, it is concluded that ZnO is a novel sorbent for the removal of As(III) from aqueous solutions.

Conclusion

ZnO nanorods have been successfully synthesized from zinc acetate using KOH as a reducing agent at room temperature. The morphological studies were conducted using SEM indicating that the As(III) adsorption was done on the surface of the adsorbent. Pseudo-first-order, pseudo-second-order and intraparticle diffusion kinetic models were used to describe the kinetic data and the rate constants were evaluated. The result of the kinetic study shows that the adsorption of As(III) could be described by the pseudo-second-order equation. The equilibrium behavior of As(III) with a stronger

affinity toward ZnO nanorods could be fitted very well by the Langmuir isotherm. The thermodynamic functions were calculated, and it can be concluded that the adsorption of As(III) over ZnO nanorods is an endothermic and spontaneous process. Hence, it may be concluded that ZnO nanorods exhibit as a good adsorbent for the treatment of aqueous solutions containing As(III) ions.

References

1. Gupta VK, Jain R, Nayak A, Agarwal S, Shrivastava M (2011) Removal of the hazardous dye—tartrazine by photodegradation on titanium dioxide surface. Mater Sci Eng 31:1062–1067
2. Gupta VK, Saini VK, Jain N (2005) Adsorption of As(III) from aqueous solutions by iron oxide-coated sand. J Colloid Interface Sci 288:55–60
3. Gupta VK, Ali I, Saini VK (2006) Adsorption of 2, 4-D and carbofuran pesticides using fertilizer and steel industry wastes. J Colloid Interface Sci 299:556–563
4. Gupta VK, Mittal A, Gajbe V, Mittal J (2008) Adsorption of basic fuchsin using waste materials—bottom ash and deoiled soya—as adsorbents. J Colloid Interface Sci 319:30–39
5. Gupta VK, Singh P, Rahman N (2004) Adsorption behavior of Hg(II), Pb(II), and Cd(II) from aqueous solution on Duolite C-433: a synthetic resin. J Colloid Interface Sci 275:398–402
6. Gupta VK, Ali I, Saini VK (2004) Removal of chlorophenols from wastewater using red mud: an aluminum industry waste. Environ Sci Technol 38:4012–4018
7. Gupta VK, Gupta B, Rastogi A, Agarwal S, Nayak A (2011) Pesticides removal from waste water by activated carbon prepared from waste rubber tire. Water Res 45:4047–4055
8. Gupta VK, Nayak A, Agarwal S (2015) Bioadsorbents for remediation of heavy metals: current status and their future prospects. Environ Eng Res 20:1–18
9. Gupta VK, Nayak A, Agarwal S, Tyagi I (2014) Potential of activated carbon from waste rubber tire for the adsorption of phenolics: effect of pre-treatment conditions. J Colloid Interface Sci 417:420–430
10. Gupta VK, Goyal RN, Sharma RA (2008) Anion recognition using newly synthesized hydrogen bonding disubstituted phenylhydrazone-based receptors: poly (vinyl chloride)-based sensor for acetate. Talanta 76:859–864
11. Gupta VK, Pathania D, Agarwal S, Sharma S (2013) Removal of Cr(VI) onto Ficus carica biosorbent from water. Environ Sci Pol Res 20:2632–2644
12. Gupta VK, Karimi-Maleh H, Sadegh R (2015) Simultaneous determination of hydroxylamine, phenol and sulfite in water and waste water samples using a voltammetric nanosensor. Int J Ele Sci 10:303–316
13. Saravanan R, Gupta VK, Prakash T, Narayanan V, Stephen A (2013) Synthesis, characterization and photocatalytic activity of novel Hg doped ZnO nanorods prepared by thermal decomposition method. J Mol Liq 178:88–93
14. Saravanan R, Thirumal E, Gupta VK, Narayanan V, Stephen A (2013) The photocatalytic activity of ZnO prepared by simple thermal decomposition method at various temperatures. J Mol Liq 177:394–401
15. Saravanan R, Prakash T, Gupta VK, Stephen A (2014) Tailoring the electrical and dielectric properties of ZnO nanorods by substitution. J Mol Liq 193:160–165
16. Saravanan R, Gupta VK, Edgar M, Gracia F (2014) Preparation and characterization of V_2O_5/ZnO nanocomposite system for photocatalytic application. J Mol Liq 198:409–412
17. Karmacharya MS, Gupta VK, Tyagi I, Shilpi A, Jha VK (2016) Removal of As(III) and As(V) using rubber tire derived activated carbon modified with alumina composite. J Mol Liq 216:836–844
18. Gupta VK, Ali I, Saini VK, Gerven TV, Bruggen VB, Vandecasteele C (2005) Removal of dyes from wastewater using bottom ash. Ind Eng Chem Res 44:3655–3664
19. Gupta VK, Ali I, Saleh TA, Nayak A, Agarwal S (2012) Chemical treatment technologies for waste-water recycling-an overview. RSC Adv 2:6380–6388
20. Gupta VK, Carrott PJM, Ribeiro C, Suhas MML (2009) Low-cost adsorbents: growing approach to wastewater treatment a review. Crit Rev Environ Sci Technol 39:783–842
21. Gupta VK, Jain R, Nayak A, Agarwal S, Shrivastava M (2011) Removal of the hazardous dye-Tartrazine by photodegradation on titanium dioxide surface. Mater Sci Eng, C 31:1062–1067
22. Gupta VK, Jain R, Saleh TA, Nayak A, Malathi S, Agarwal S (2011) Equilibrium and thermodynamic studies on the removal and recovery of Safranine-T dye from industrial effluents. Sep Sci Technol 46:839–846
23. Gupta VK, Kumar R, Nayak A, Saleh TA, Barakat MA (2013) Adsorptive removal of dyes from aqueous solution onto carbon nanotubes: a review. Adv Colloid Interface Sci 193–194:24–34
24. Gupta VK, Jain R, Mittal A, Saleh TA, Nayak A, Agarwal S, Sikarwar S (2012) Photo-catalytic degradation of toxic dye amaranth on TiO 2/UV in aqueous suspensions. Mater Sci Eng 32:12–17
25. Mittal A, Mittal J, Malviya A, Kaur D, Gupta VK (2010) Decoloration treatment of a hazardous triarylmethane dye, light green SF (Yellowish) by waste material adsorbents. J Colloid Interface Sci 342:518–527
26. Mittal A, Mittal J, Malviya A, Gupta VK (2010) Removal and recovery of Chrysoidine Y from aqueous solutions by waste materials. J Colloid Interface Sci 344:497–507
27. Gupta VK, Shrivastava AK, Jain N (2001) Biosorption of chromium (VI) from aqueous solutions by green algae Spirogyra species. Water Res 35:4079–4085
28. Gupta VK, Agarwal S, Saleh TA (2011) Mater. Synthesis and characterization of alumina-coated carbon nanotubes and their application for lead removal. J Hazard 185:17–23
29. Gupta VK, Rastogi A (2008) Biosorption of lead from aqueous solutions by green algae Spirogyra species: kinetics and equilibrium studies. J Hazard Mater 152:407–414
30. Gupta VK, Kumar R, Nayak A, Saleh TA, Barakat MA (2013) Adsorptive removal of dyes from aqueous solution onto carbon nanotubes: a review. Adv Colloid Interface Sci 193:24–34
31. Gupta VK, Rastogi A, Nayak A (2010) Adsorption studies on the removal of hexavalent chromium from aqueous solution using a low cost fertilizer industry waste material. J Colloid Interface Sci 342:135–141
32. Martinson CA, Reddy KJ (2009) Adsorption of arsenic(III) and arsenic(V) by cupric oxide nanoparticles. J Colloid Interface Sci 336:406–411

33. Smith AH, Lopipero PA, Bates MN, Steinmaus CM (2002) Arsenic epidemiology and drinking water standards. Science 296:2145–2146

34. Mohan D, Pittman CU (2007) Arsenic removal from water/wastewater using adsorbents—a critical review. J Hazard Mater 142:1–53

35. Sharma VK, Sohn M (2009) Aquatic arsenic: toxicity, speciation, transformations, and Remediation. Environ Int 35:743–759

36. Choong TSY, Chuah TG, Robiah Y, Koay FLG, Azni I (2007) Arsenic toxicity, health hazards and removal techniques from water: an overview. Desalination 217:139–166

37. Sancha AM (2000) Removal of arsenic from drinking water supplies: chile experience. Water Supply 18:621–625

38. Viraraghavan T, Subramanian KS, Tanjore S (1996) Removal of arsenic in drinking water by manganeseegreensand filtration, oxide-ccoated sand filtration and ion exchange treatment. Adv Filtr Sep Technol 10:502–507

39. Madaeni SS, Mansourpanah Y (2003) COD removal from concentrated wastewater using membranes. Filtr Separat 40:40–46

40. Qin JJ, Wai MN, Oo MH, Wong FS (2002) A feasibility study on the treatment and recycling of a wastewater from metal plating. J Membr Sci 208:213–221

41. Lai CL, Lin SH (2003) Electro coagulation of chemical mechanical polishing (CMP) wastewater from semiconductor fabrication. J Chem Eng 95:205–211

42. Li XM, Liao DX, Xu XQ, Qi Y, Zeng GM, Wei Z, Liang G (2008) Kinetic studies for the biosorption of lead and copper ions by Penicillium simplicissimum immobilized within loofa sponge. J Hazard Mater 159:610–615

43. Baysal Z, Cınar E, Bulut Y, Alkan H, Dogru M (2009) Equilibrium and thermodynamic studies on biosorption of Pb(II) onto Candida albicans biomass. J Hazard Mater 161:62–67

44. Tajar AF, Kaghazchi T, Soleimani M (2009) Adsorption of cadmium from aqueous solutions on sulfurized activated carbon prepared from nut shells. J Hazard Mater 165:1159–1164

45. Maji SK, Pal M, Pal T, Adak A (2007) Adsorption thermodynamic of As on laterite soil. J Surf Sci Technol 22:161–176

46. Sari A, Uluozlu OD, Tuzen M (2011) Equilibrium, thermodynamic and kinetic investigations on biosorption of arsenic from aqueous solution by algae (Maugeotia genuflexa) biomass. J Chem Eng 167:155–161

47. Uluozlu OD, Sari A, Tuzen M, Soylak M (2008) Biosorption of Pb(II) and Cr(III) from aqueous solution by lichen (Parmelina tiliaceae) biomass. Bioresour Technol 99:2972–2980

48. Sari A, Tuzen M, Uluozlu OD, Soylak M (2007) Biosorption of Pb(II) and Ni(II) from aqueous solution by lichen (Cladonia furcata) biomass. J Biochem Eng 37:151–158

49. Boddu VM, Krishnaiah A, Talbortt JL, Smith ED, Haasch R (2008) Removal of arsenic (III) and arsenic (V) from aqueous medium using chitosan-coated biosorbent. Water Res 42:633–642

50. Ghaedi M, Khafri ZH, Asfaram A, Goudarzi A (2016) Response surface methodology approach for optimization of adsorption of Janus Green B from aqueous solution onto ZnO/Zn(OH)2-NP-AC: kinetic and isotherm study. Spectrochima Acta A 152:233–240

51. Jamshidi M, Ghaedi M, Dashtian K, Hajati S, Bazrafshan AA (2016) Sonochemical assisted hydrothermal synthesis of ZnO: Cr nanoparticles loaded activated carbon for simultaneous ultrasound-assisted adsorption of ternary toxic organic dye: derivative spectrophotometric, optimization, kinetic and isotherm study. Ultrason Sonochem 32:119–131

52. Ghaedi M, Ansari A, Habibi MH, Asghari AR (2014) Removal of malachite green from aqueous solution by zinc oxide nanoparticle loaded on activated carbon: kinetics and isotherm study. J Ind Eng Chem 20:17–28

53. Dil EA, Ghaedi M, Ghaedi AM, Asfaram A, Goudarzi A, Hajati S, Soylak M, Shilpi A, Gupta VK (2016) Modeling of quaternary dyes adsorption onto ZnO–NR–AC artificial neural network: analysis by derivative spectrophotometry. J Ind Eng Chem 34:186–197

54. Paritam KD, Ray AK, Sharma VK, Millero FJ (2004) Adsorption of arsenate and arsenite on titanium dioxide suspensions. J Colloid Interface Sci 278:270–275

55. Qi L, Xu Z (2004) Lead sorption from aqueous solutions on chitosan nanoparticles. Colloid Surf A 251:183–190

56. Sheela T, Nayak YA, Viswanatha R, Basavanna S, Venkatesha TG (2012) Kinetics and thermodynamics studies on the adsorption of Zn(II), Cd(II) and Hg(II) from aqueous solution using zinc oxide nanoparticles. Powder Technol 217:163–170

57. Ciftci TD, Henden E (2015) Nickel/nickel boride nanoparticles coated resin: a novel adsorbent for arsenic(III) and arsenic(V) removal. Powder Technol 269:470–480

58. Hang C, Li Q, Gao S, Shang JK (2012) As(III) and As(V) adsorption by hydrous zirconium oxide nanoparticles synthesized by a hydrothermal process followed with heat treatment. Ind Eng Chem Res 51:353–361

59. Zhang S, Niu H, Cai Y, Zhao X, Shi Y (2010) Arsenic and arsenate adsorption on coprecipitated bimetal oxide magnetic nanomaterials: mnFeO$_4$ and CoFe$_2$O$_4$. J Chem Eng 158:599–607

60. Lagergren S (1898) Zur theorie der sogenannten adsorption geloster stoffe. K Seven Vetenskapsakad Handl 24:1–39

61. Ho YS, McKay G, Wase DAJ, Foster CF (2000) Study of the sorption of divalent metal ion onto peat. Adsorpt Sci Tech 18:639–650

62. Weber WJ, Morris JC (1963) Kinetics of adsorption on carbon from solution. J Sanit Eng Div Am Soc Civil Eng 89:31–60

63. Langmuir I (1918) The adsorption of gases on plane surfaces of glass, mica and Platinum. J Am Chem Soc 40:1361–1403

64. Freundlich HMF (1906) Uber die adsorption in lasugen. Z Phys Chem 57:385–470

65. Samsuri AW, Zadeh FS, Seh-Bardan BJ (2013) Adsorption of As(III) and As(V) by Fe coated biochars and biochars produced from empty fruit bunch and rice husk. J Environ Chem Eng 1:981–988

66. Jesus C, Louis EG, Jacqueline G, Monica C, Meera J, Cameron G, Eubanks TM, Parsons JG (2016) Removal of arsenic from water using synthetic Fe7S8 nanoparticles. Chem Eng J 290:428–437

67. Vieira BRC, Pintor AMA, Boaventura RAR, Botelho CMS, Santos SCR (2017) Arsenic removal from water using iron-coated seaweeds. J Environ Manage 192:224–233

68. Namor AFDD, Hakawati NA, Hamdan WA, Soualhi R, Samira K, Liliana V (2017) Calix [4] pyrrole for the removal of arsenic(III) and arsenic(V) from water. J Hazard Mater 326:61–68

69. Chen B, Zhu Z, Ma J, Qiu Y, Chen J (2013) Surfactant assisted CeeFe mixed oxide decorated multiwalled carbon nanotubes and their arsenic adsorption performance. J Mater Chem A 1:11355–11367

70. Baikousi M, Georgiou Y, Daikopoulos C, Bourlinos AB, Filip J, Zboril R, Deligiannakis Y, Karakassides MA (2015) Synthesis and characterization of robust zero valent iron/mesoporous carbon composites and their applications in arsenic removal. Carbon 93:636–647